Diamond & Related Materials 20 (2011) 343–350

Contents lists available at ScienceDirect

Diamond & Related Materials

journal homepage: www.elsevier.com/locate/diamond

Fabrication of CNTs with controlled diameters and their applications as electrocatalyst supports for DMFC☆

An-Ya Lo [a,b], Ningya Yu [a,1], Shing-Jong Huang [c], Chin-Te Hung [a], Shou-Heng Liu [a,2], Zhibin Lei [a,3], Cheng-Tzu Kuo [d,*], Shang-Bin Liu [a,e,**]

[a] Institute of Atomic and Molecular Sciences, Academia Sinica, Taipei 10617, Taiwan
[b] Department of Material Science and Engineering, National Chiao Tung University, Hsingchu 30010, Taiwan
[c] Department of Chemistry, National Taiwan University, Taipei 10617, Taiwan
[d] Institute of Materials and System Engineering, Ming Dao University, Changhua 52345, Taiwan
[e] Department of Chemistry, National Taiwan Normal University, Taipei 11677, Taiwan

ARTICLE INFO

Available online 19 January 2011

Keywords:
Carbon nanotube
Templating synthesis
Chemical vapor deposition
Hexagonal mesoporous silica
Electrocatalyst
Direct methanol fuel cell

ABSTRACT

A facile synthesis procedure based on chemical vapor deposition (CVD) process has been developed to fabricate carbon nanotubes (CNTs) with controlled diameters and high yields utilizing Fe-containing ordered hexagonal mesoporous silicas (HMSs) such as MCM-41 and SBA-15 having varied pore sizes as the catalysts as well as the templates. It is found that unlike Fe/HMS catalysts prepared by co-precipitation method, samples prepared by the impregnation method gave rise to multi-wall CNTs with uniform diameters, which were largely dictated by the pore size of the Fe/HMS catalysts. Among these uniform MWCNTs, sample with a larger diameter (≥8 nm) was found to be more favorable as support for Pt catalyst, leading to a homogeneous dispersion of metal nanoparticles. Consequently, the Pt/CNT electrocatalysts so prepared gave rise to superior methanol oxidation activities as well as tolerances for CO poisoning compared to Pt supported on commercial single-wall CNT (Pt/SWCNT) and XC-72 activated carbon (Pt/XC-72) having a similar metal loading.

1. Introduction

Recent developments in fabrication of porous carbon supports with high surface areas and controllable morphologies have received considerable attention in R&D of supported electrocatalysts for direct methanol fuel cells (DMFCs) and proton-exchange membrane fuel cells (PEMFCs), which have been considered as the most prominent candidates for next-generation portable power sources [1–4]. Highly dispersed noble metal (Pt, Ru) nanoparticles (NPs) supported on conductive materials with high surface areas, such as carbon blacks [5,6], ordered mesoporous carbons (OMCs) [7–13], and carbon nanotubes (CNTs) [14–18], are pertinent anodic/cathodic electrocatalysts for DMFCs and PEMFCs. Among them, CNTs have received considerable attention due to their unique one-dimensional nanostructure and superior electrical conductivity. Aside from the most common electrocatalysts for DMFCs, such as Pt/Ru supported on commercial Vulcan XC-72 carbon black, many attempts have been made utilizing CNTs as catalyst supports [14–23]. However, while majority of past research efforts have been devoted in optimizing the metal dispersion on single-wall (SW) and multi-wall (MW) CNTs aiming to promote their electrocatalytic performances and durability, practically no report had been focused on the diameter size of the CNT supports.

In general, the methodologies invoked in controlling the diameter of CNTs during chemical vapor deposition (CVD) process may be classified into two main categories, namely by controlling the processing parameters and by employing an auxiliary template. For the former, it has been reported that parameters such as the carrier gas/carbon source flow rate, plasma intensity, morphology of the catalyst, precursor compositions, and duration of treatment etc. have considerable effects on the diameter of the final CNT products [24–28]. In contrast to such sophisticated adjustment of processing parameters, the use of an auxiliary template appears to be more advantageous in fabricating CNTs with tailorable diameters. For examples, zeolites [29] and anodic metal oxides [30–36] have been utilized as hard templates during the CVD process to fabricate CNTs with uniform diameters. In this case, the diameters of the CNTs so synthesized are largely dictated by the pore size of template used. However, since it is rather difficult to prepare anodic metal oxides

☆ Presented at NDNC 2010, the 4th International Conference on New Diamond and Nano Carbons, Suzhou, China.

* Corresponding author. Fax: +886 4 8879050.
** Correspondence to: S.-B. Liu, Institute of Atomic and Molecular Sciences, Academia Sinica, Taipei 10617, Taiwan. Fax: +886 2 23620200.
E-mail addresses: kuoct@mdu.edu.tw (C.-T. Kuo), sbliu@sinica.edu.tw (S.-B. Liu).
[1] Present address: Institute of Fine Catalysis and Synthesis and Key Lab of Sustainable Resources Processing and Advanced Materials of Hunan Province, Hunan Normal University, Changsha 410081, China.
[2] Present address: Department of Chemical and Materials Engineering, National Kaohsiung University of Applied Sciences, Kaohsiung 80778, Taiwan.
[3] Present address: Department of Chemical & Biomolecular Engineering, National University of Singapore, Singapore.

0925-9635/$ – see front matter © 2011 Elsevier B.V. All rights reserved.
doi:10.1016/j.diamond.2011.01.002

with uniform pore sizes less than 25 nm, majority of the CNTs so fabricated possess diameters exceeding 25 nm [36]. On the other hand, CNTs fabricated by using microporous zeolites as templates mostly have diameters less than 1 nm. In view of the fact that the diameter of CNT is one of the key parameters affecting their physical properties, it is highly desirable to develop a facile synthesis route to fabricate CNTs with tunable diameters within the range of 1–25 nm.

Ordered hexagonal mesoporous silicas (HMSs), especially those possessing straight mesoporous channels with uniform pore sizes in the range of 2–50 nm, such as MCM-41 [37] and SBA-15 [38,39] seem to represent the ideal templates to meet the aforementioned demand [40]. It is worth mentioning that although various ordered mesoporous silicas have been invoked for the preparation of CNTs, they were mostly employed as supports to disperse or to limit the size and structure of the catalytic metal nanoparticles [41–48], overlooking the templating function of the porous substrates. We report herein a facile synthesis route to synthesize CNTs with tunable diameters and high yields by using Fe-containing HMSs as catalyst templates. The resultant CNTs with varied diameters were used as supports to prepare various Pt/CNT anodic electrocatalysts for DMFC applications and their catalytic performances during methanol oxidation reaction (MOR) were evaluated and compared with a Pt/XC-72 catalyst (12.5 wt.% Pt on Vulcan XC-72).

2. Experimental

2.1. Preparation of Fe-containing HMSs

Three types of ordered HMSs, namely MCM-41, SBA-15, and pore expanded SBA-15 (denoted as PE-SBA-15) were synthesized by known recipes reported previously [37–39,49]. Iron catalyst was loaded onto the HMSs *via* either co-precipitation or impregnation methods. For the former, typically ca. 0.4 g of $Fe(NO_3)_3$ was stirring with 1.0 g of the target HMS material for 0.5 h in deionized water (20 mL), followed by filtering and drying at 373 K, then subjected to reduction treatment under H_2 at 773 K for 3 h. The Fe-containing HMSs so obtained from the siliceous MCM-41 and SBA-15 are denoted as Fe(co)/MCM-41 and Fe(co)/SBA-15, respectively. In the case of loading Fe catalyst by the impregnation method, proper amount of Fe $(NO_3)_3$ (ca. one-half pore volume of the corresponding support) was dissolved in 20 mL deionized water, followed by adding 1.0 g of the target HMS. After being stirred for 0.5 h, the suspension was dried under vacuum. The obtained product was further stirred in presence of dichloromethane (CH_2Cl_2) to facilitate migration of Fe precursors into the hydrophilic channels of the HMSs [50], followed by removal of the CH_2Cl_2 solvent by evacuation. The above procedure was repeated once and the final product was subjected to reduction treatment carried out by first slowly ramping (2 K/min) the temperature to 373 K under dried Ar, kept at the same temperature for 3 h, followed by reduction under H_2 environment before a mixture of acetylene (C_2H_2) and hydrogen (H_2) was injected for CNTs growth. The Fe-containing HMSs so derived from the siliceous MCM-41, SBA-15, and PE-SBA-15 are denoted as Fe(im)/MCM-41, Fe(im)/SBA-15, and Fe(im)/PE-SBA-15, respectively.

2.2. Fabrication of CNTs with uniform diameters

CNTs with varied diameters were prepared by a CVD method similar to that reported earlier for the nano-sized tubular carbons (i.e., CMTs) [51]. In brief, the syntheses were carried out in a home-made quartz reactor using various Fe-containing HMSs as templates. Typically, after loading ca. 0.5 g of the fresh Fe-containing HMS in the reactor, the system was first gradually heated (1 K/min) to 873 K under vacuum, followed by injecting a stream of C_2H_2/H_2 gas mixture at a flow rate of 50/50 sccm/sccm for 40 min under a pressure of *ca.* 2 kPa. The resultant product was stirred with excess aqueous HF solution (1 M, 50% ethonal–50% H_2O) for 24 h to remove the silica template and Fe species, followed by filtering and drying under vacuum to obtain the final multi-wall carbon nanotube (MWCNT) materials.

2.3. Preparation of Pt/CNT electrocatalysts

To explore the effect of tube diameter on the performances of various CNTs as catalyst supports for DMFC at anode, typically ca. 0.2 g of the selected home-made CNT was individually suspended in 10 mL of H_2PtCl_6 aqueous solution (0.04 M) at room temperature. After removing water under reduced pressure, the obtained solid was treated at 523 K for 0.5 h under H_2 atmosphere to provoke reduction

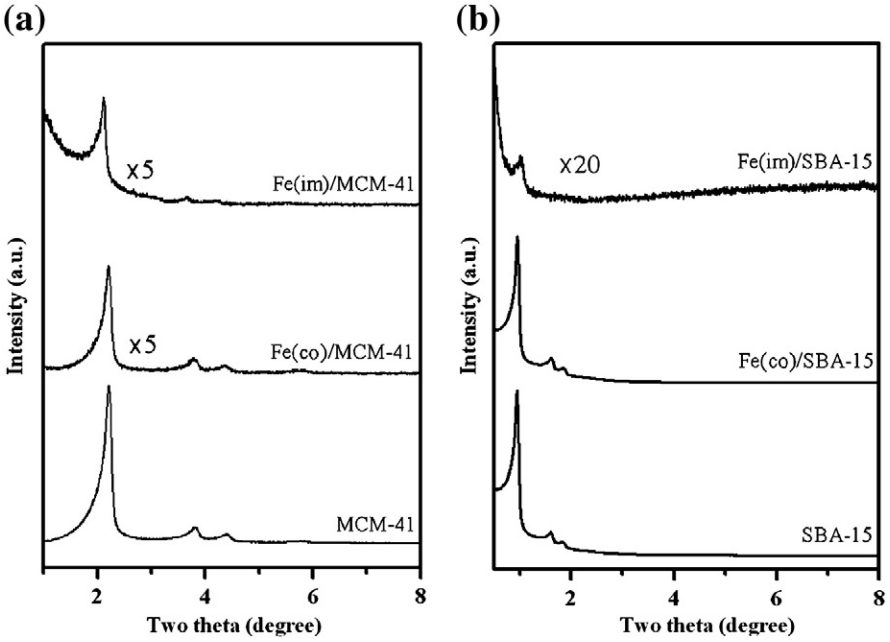

Fig. 1. Small-angle XRD patterns of siliceous and Fe-containing HMSs; (a) MCM-41 and (b) SBA-15.

of $PtCl_6^{2-}$ to Pt nanoparticles. For comparison purpose, two commercial products, namely the Vulcan XC-72 carbon black (Cabot Corp.) and single-wall CNTs (SWCNTs; Nano-C Inc.) were also adopted as supports to fabricate Pt-containing electrocatalysts with similar metal loading *via* the aforementioned procedures.

2.4. Materials characterization and electrocatalytic tests

Powder X-ray diffraction (XRD) patterns of various samples were recorded on a Philips X' PERT-Pro-MPD diffractometer using the CuKα radiation (λ = 1.542 Å). All nitrogen adsorption/desorption isotherm measurements were carried out at 77 K on a Quantachrome Autosorb-1 sorptometer. Prior to the measurement, each sample was outgassed at 473 K under vacuum (10^{-6} Torr) overnight. The surface area of each sample was derived by the BET method, and its pore size distribution (PSD) was calculated from the adsorption branch of the isotherm using the Barrett–Joyner–Halenda (BJH) method. Transmission electron microscopy (TEM) studies were performed on a JEOL JEM-2100 F microscope operated at 200 kV. Each sample was ultrasonicated for 15 min in ethanol before introducing it onto the carbon-coated copper grids. The metal (Fe and Pt) contents in various samples were determined by thermal gravimetric analyses (TGA; Netzsch TG-209).

The electrochemical active surfaces (EASs), electrocatalytic performances, and stability of various supported Pt/C catalysts were evaluated on an Autolab PGSTAT30 galvanostat/potentiostat at room temperature by using a glassy carbon thin-film as the working electrode, Pt wire as the counter electrode, and Ag/AgCl as the reference electrode. Typically, the glassy carbon thin-film electrode was prepared by first adding ca. 10 mg of Pt-loaded CNTs sample into 5 mL of deionized water, followed by ultrasonic treatment for 0.5 h. Next, ca. 20 μL of the resultant suspension mixture was withdrawn and injected onto the glassy carbon electrode (diameter ca. 5 mm), followed by drying in air at 333 K for 1 h. Finally, ca. 20 μL of 1% Nafion (DuPont) solution was added as a binder under N_2 environment. Prior to each cyclic voltammetry (CV) measurement, the electrolytic

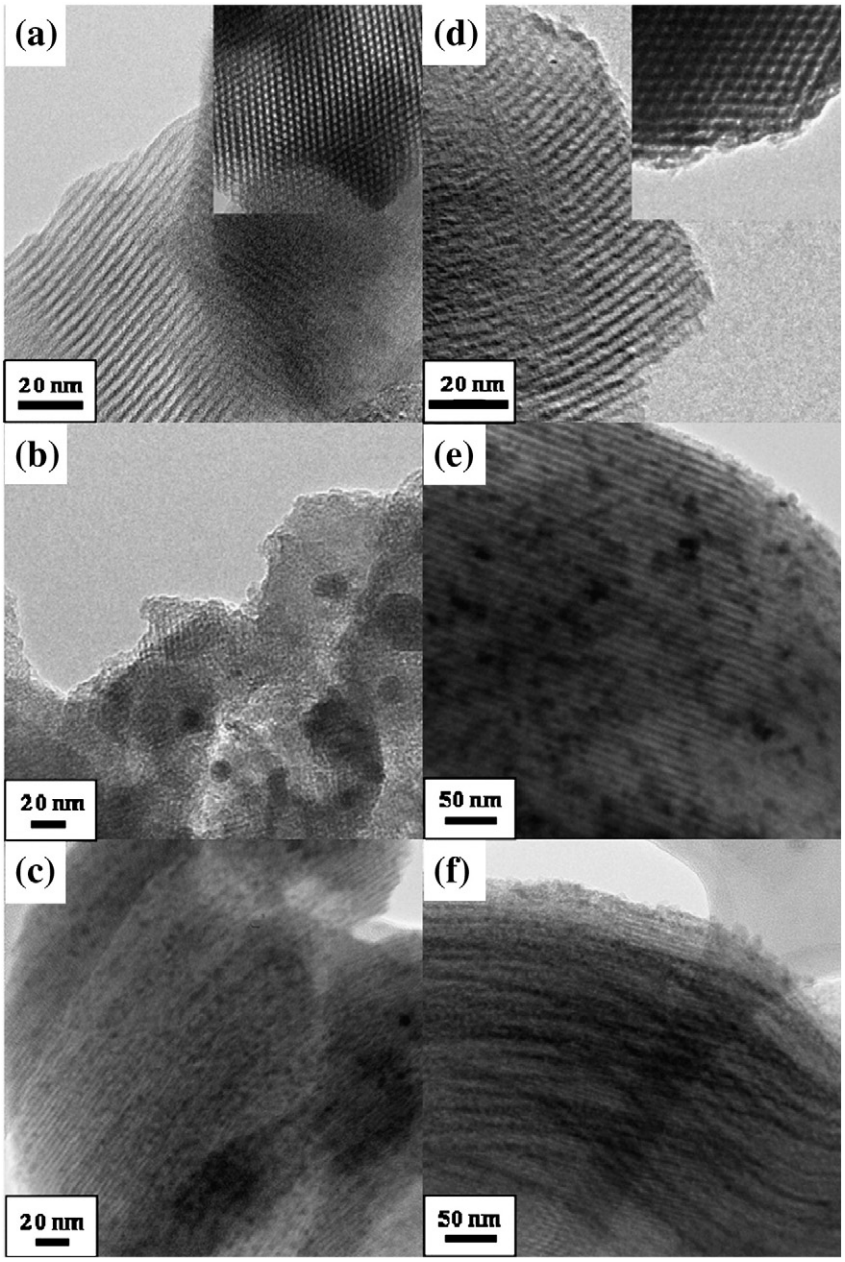

Fig. 2. TEM images of (a) siliceous MCM-41, (b) Fe(co)/MCM-41, (c) Fe(im)/MCM-41, (d) siliceous SBA-15, (e) Fe(co)/SBA-15, and (f) Fe(im)/SBA-15.

solution was purged with purified N_2 gas (99.9%) for at least 0.5 h to remove the dissolved oxygen. The EAS and electrooxidation of methanol (MeOH) was carried out with an electrolyte of H_2SO_4 (1.0 M) and H_2SO_4 (0.5 M)/MeOH (1 M) solution, respectively, between −0.2 and 1.0 V at a 10 mV/s scanning rate. Prior to each measurement, the corresponding working electrode was scanned by CV in H_2SO_4 (1.0 M) at room temperature till it reached a steady state. In addition, chronoamperometry (CA) measurements were also carried out for assessment of catalyst stability. The corresponding working electrode was measured under a constant (0.6 V) anodic potential with an electrolyte of H_2SO_4 (0.5 M)/MeOH (1 M) during these experiments, Note that all of the above electrochemical experiments were conducted under purging N_2 condition.

3. Results and discussion

3.1. Effect of Fe loading method for Fe/HMS on CNT diameter control

Fig. 1 displays the XRD patterns of the parent siliceous MCM-41 and SBA-15 mesoporous silicas as well as their corresponding Fe-containing counterparts prepared by different methods. Both the siliceous SBA-15 and MCM-41 showed three well-resolved diffraction peaks that may be indexed as (100), (110), and (200) reflections associated with the well-ordered hexagonal arrays of mesopores [37–39]. The method applied in loading Fe onto the mesoporous silica appears to have significant effects on the mesostructure of the Fe-containing HMSs. Clearly, the Fe(co)/MCM-41 and Fe(co)/SBA-15 samples prepared *via* the co-precipitation method tend to retain the ordered structures of their parent silica supports, although substantial decreases in intensities of the diffraction peaks were evident. On the other hand, Fe-containing HMSs prepared by the impregnation method, i.e., Fe(im)/MCM-41 and Fe(im)/SBA-15, exhibited a main d_{100} diffraction peak with nearly diminishing higher order (d_{110} and d_{200}) peaks. Thus, unlike Fe(co)/HMSs, incorporation of Fe catalyst by impregnation method tends to lose the integrity of long-range structural ordering of the siliceous HMSs, as observed for Fe(im)/HMSs in Fig. 1. The same conclusion may be drawn from the TEM results in Fig. 2. It is worth pointing out that a parallel alignment of pore channels should be observed when the electron beam was introduced perpendicular to the channel axis (Fig. 2a and d), whereas hexagonal packing of cylindrical mesopores prevails when the electron beam was introduced along the channel axis (see insets in Fig. 2a and d). It is clear that the Fe(co)/MCM-41 (Fig. 2b) and Fe(co)/SBA-15 (Fig. 2e) samples retained the hexagonal pore systems of their respective parent silicas. However, it is also evident that the co-precipitation process invoked led to a

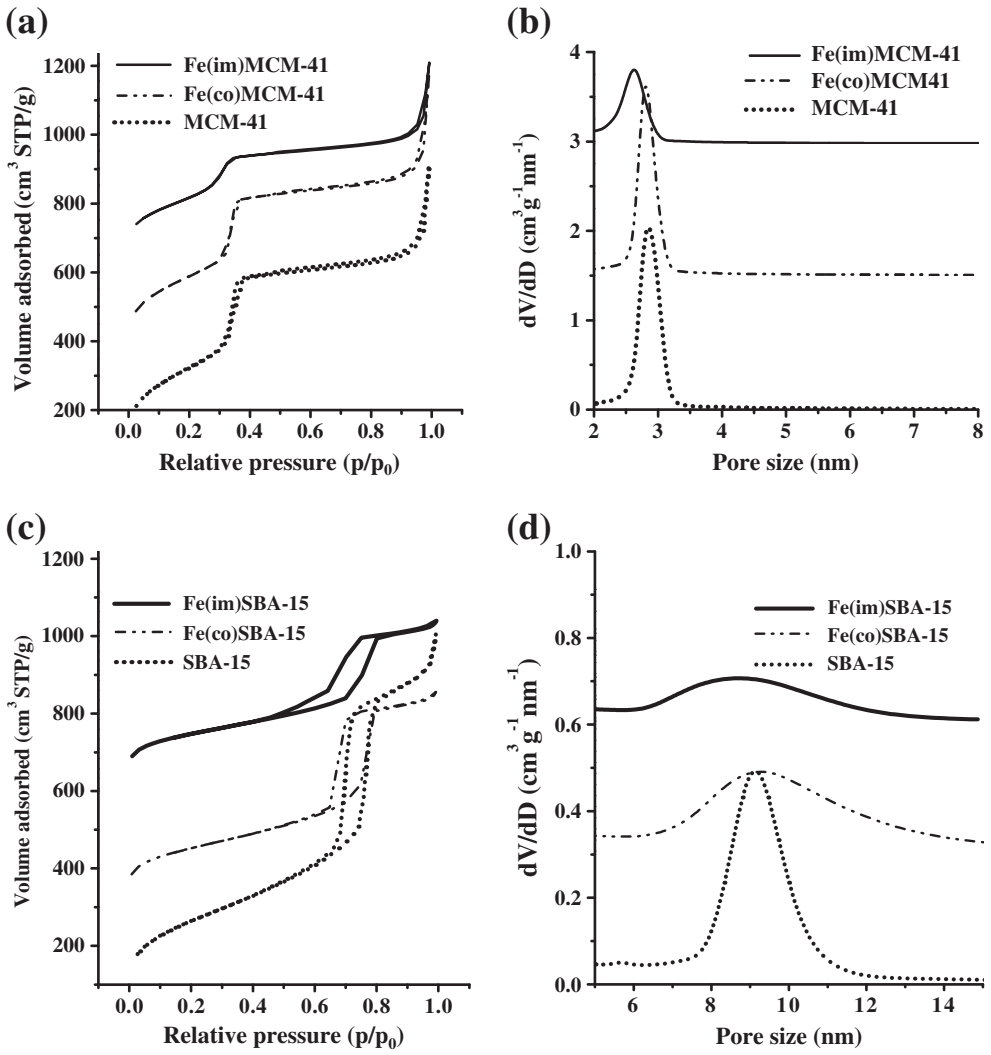

Fig. 3. Nitrogen adsorption/desorption isotherms and pore size distributions of siliceous and Fe-containing HMSs (a, b) MCM-41 and (c, d) SBA-15. The isotherms of Fe(co)/MCM-41, Fe(im)/MCM-41, Fe(co)/SBA-15, and Fe(im)/SBA-15 were shifted vertically by 300, 600, 300, and 600 cm^3 g^{-1} STP, respectively, whereas the pore size distribution curves for Fe(co)/MCM-41, Fe(im)/MCM-41, Fe(co)/SBA-15, and Fe(im)/SBA-15 were shifted vertically by 1.5, 3.0, 0.3, and 0.6 cm^3 g^{-1} nm^{-1}, respectively.

heterogeneous dispersion of Fe particles on the external surfaces of the mesoporous silica supports.

On the other hand, while the TEM images of Fe(im)/MCM-41 (Fig. 2c) and Fe(im)/SBA-15 (Fig. 2f) seemingly showed well ordered hexagonal pore systems, incorporation of Fe onto HMSs by impregnation method led to partial formation of Fe nanorods within the pore channels. In this context, the diameter of these Fe nanorods should be constrained by the pore aperture of the HMS supports, leading to substantial reductions in their scattering contrasts [52–54]. Thus, the notable decrease in the intensity of the main d_{100} diffraction peak and the disappearance of the higher order peaks observed for Fe(im)/MCM-41 and Fe(im)/SBA-15 in Fig. 1 may be ascribed due to the presence of Fe nanorods in the mesochannels of the silica supports rather than degradation of their mesostructures.

Nitrogen adsorption/desorption isotherms obtained from various samples are shown in Fig. 3 together with their corresponding PSDs. The textural properties of various samples were also depicted in Table 1. Comparing with their parent silica materials, Fe-containing HMSs typically showed smaller pore volumes and broader PSDs regardless of the method adopted in incorporating the Fe catalyst. While the Fe(co)/MCM-41 and Fe(co)/SBA-15 samples showed similar pore sizes (D_{BJH}) compared to their respective silica supports, slight decreases in pore volumes (V_p) and BET surface areas (S_{BET}) were observed after loading the Fe catalyst (Table 1). On the other hand, notable decreases in D_{BJH}, V_p, and S_{BET} were observed for the Fe(im)/MCM-41 and Fe(im)/SBA-15 compared to their respective siliceous counterparts before loading the Fe catalyst (Table 1). These observations are in line with the aforediscussed XRD and TEM results, that is, incorporation of the Fe catalyst by impregnation method led to the formation of Fe nanorods within the pore channels of the HMSs, whereas samples prepared using the co-precipitation method resulted in an inhomogeneous dispersion of Fe nanoparticles (typically, ca. 20 nm in size) on the external surfaces of the HMSs.

Typical TEM micrographs of CNTs synthesized by CVD process using various Fe-containing HMSs as catalysts are depicted in Fig. 4. In the cases of using the Fe(co)/MCM-41 and Fe(co)/SBA-15 supported catalysts, the obtained CNTs typically possessed an average diameter greater than 5 (Fig. 4a) and 10 nm (Fig. 4c), respectively, which were apparently greater than the pore sizes of their corresponding catalyst templates (2.8 and 9.2 nm, respectively; see Table 1). These observations are in parallel to the existing literature reports [42,43,47]. In contrast, the CNTs synthesized using the Fe(im)/MCM-41 and Fe(im)/SBA-15 catalysts were found to exhibit a uniform diameter of ca. 3 (Fig. 4b) and 8 (Fig. 4d) nm, respectively, in close resemblance with the average pore sizes of the corresponding Fe-containing HMSs (2.6 and 8.6 nm, respectively; see Table 1). The above results indicate that Fe-containing HMSs so designed and prepared can be employed not only as catalysts to fabricate CNTs but also as templates to manipulate the diameters of the synthesized CNTs. To further verify these points, an additional PE-SBA-15 sample with expanded pore size of 17.5 nm (Table 1 and Fig. 5a) was synthesized. After incorporating the Fe catalyst by impregnation method, the resultant Fe(im)/PE-SBA-15 sample was employed as catalyst (and template) to produce CNTs. As shown in Fig. 5b, the CNTs so fabricated also possessed a rather uniform diameter (ca. 17 nm) comparable to the pore size of the Fe(im)/PE-SBA-15 catalyst (17.5 nm). It is noteworthy that the CNTs produced by CVD process using the Fe-containing HMSs reported herein also exhibited superior high yields in terms of atom efficiency. For examples, a CNT yield as high as 0.3 g was obtained during a CVD duration time of 20 min using ca. 1.0 g of Fe(im)/SBA-15 as catalyst/template. Likewise, a respective CNT yield of 0.1 and 0.4 g/20 min were attained when Fe(im)/MCM-41 and Fe(im)/PE-SBA-15 were employed.

Table 1
Textural properties of various siliceous and Fe-containing HMSs.[a]

Sample	d_{100} (nm)	D_{BJH} (nm)	S_{BET} (m^2/g)	V_p (cm^3/g)
MCM-41	4.0	2.9	1153	0.97
Fe(co)/MCM-41	4.0	2.8	949	0.79
Fe(im)/MCM-41	4.2	2.6	540	0.50
SBA-15	9.4	9.1	823	1.30
Fe(co)/SBA-15	9.4	9.2	739	1.27
Fe(im)/SBA-15	8.7	8.6	498	0.64
PE-SBA-15	–	18.0	709	1.64
Fe(im)/PE-SBA-15	–	17.5	464	0.63

[a] d_{100} : d spacing measured in the (100) plane; D_{BJH} : pore diameter derived by BJH method; S_{BET} : BET surface area; V_p: pore volume.

3.2. Effect of CNT diameter on Pt dispersion and electrochemical properties

As shown above, the MWCNTs synthesized by using the Fe(im)/MCM-41, Fe(im)/SBA-15, and Fe(im)/PE-SBA-15 catalyst possess an

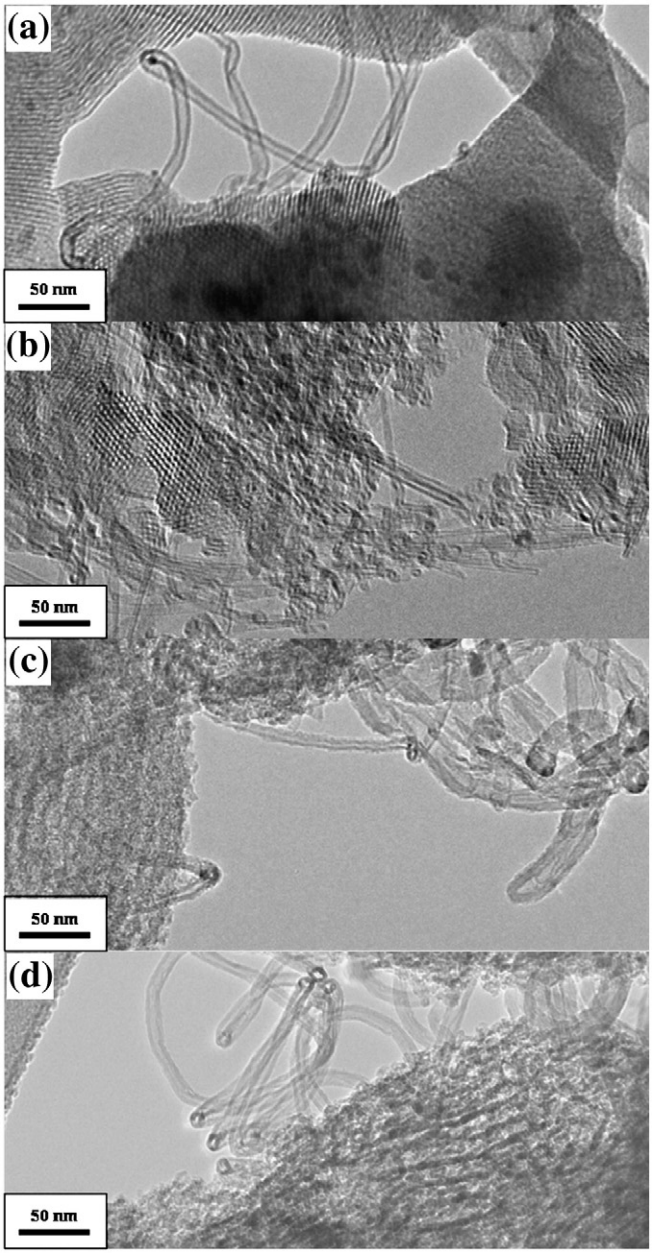

Fig. 4. TEM images of CNTs prepared using various Fe-containing HMSs; (a) Fe(co)/MCM-41, (b) Fe(im)/MCM-41, (c) Fe(co)/SBA-15, and (d) Fe(im)/SBA-15.

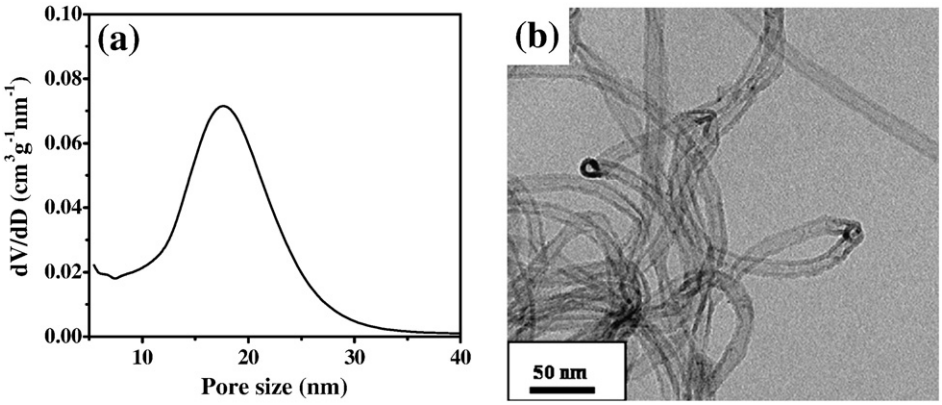

Fig. 5. (a) Pore size distribution of Fe(im)/PE-SBA-15 and (b) the TEM image of the resultant CNTs.

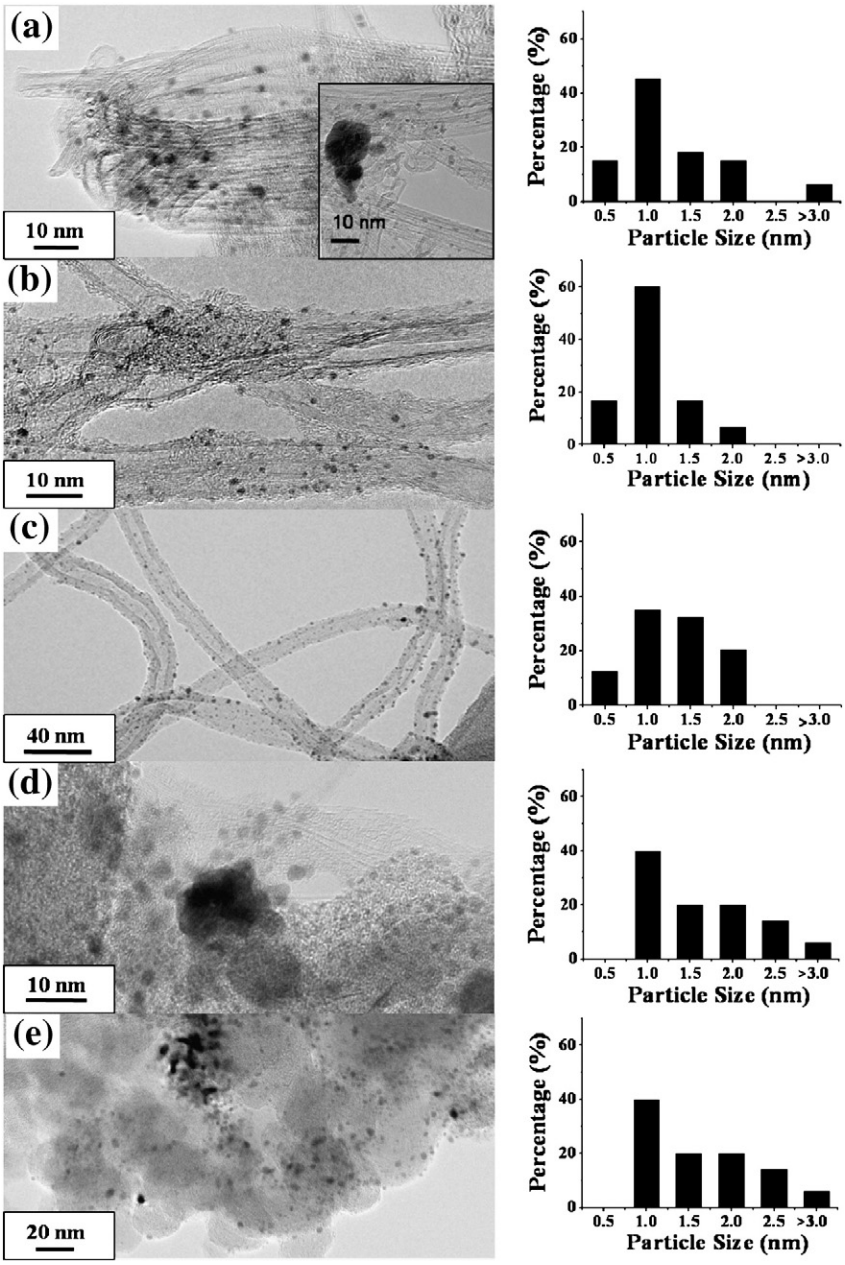

Fig. 6. (Left) TEM images and (Right) Pt particle size distribution of various Pt/C electrocatalysts; (a) Pt/CNT-d3, (b) Pt/CNT-d8, (c) Pt/CNT-d17, (d) Pt/SWCNT, and (e) Pt/XC-72.

average diameter of ca. 3, 8, and 17 nm, respectively. These CNTs with uniform diameters, together with a commercial SWCNT were subsequently used as supports for Pt catalyst, the resultant supported Pt/C catalyst samples are donated as Pt/CNT-d3, Pt/CNT-d8, Pt/CNT-d17, and Pt/SWCNT, respectively. The mean Pt particle sizes of these Pt/C samples as well as Pt/XC-72 were preliminary estimated by well-known Scherrer formula [55,56] based on the large-angle XRD (220) diffraction peak of Pt metal (not shown) occurring at 2θ of ca. 68°. Accordingly, a similar Pt particle size of ca. 2.4 nm were observed for the Pt/CNT-d17, Pt/CNT-d8, and Pt/XC-72 samples, whereas slightly larger Pt nanoparticles (>3 nm) was found for the Pt/CNT-d3 and the Pt/SWCNT samples. The Pt particle sizes in different samples were further evaluated by TEM analyses. Fig. 6 displays the resultant TEM images of various Pt/C catalysts and their corresponding histograms of Pt particle size distribution. Clearly, majority of the Pt/C samples with CNTs as supports show Pt particle size predominately in the range of 1–2 nm. However, unlike the Pt/CNT-d8 (Fig. 6b) and the Pt/CNT-d17 (Fig. 6c) samples, which showed uniform Pt dispersions typically with Pt particle size ≤2 nm, the Pt/CNT-d3 sample appeared to have lower Pt dispersion similar to that of the Pt/SWCNT and the Pt/XC-72 samples. As revealed by Fig. 6a, d, and e, Pt particles exceeding 10 nm may be identified in the latter three samples. A closer examination of the TEM profile for the Pt/CNT-d3 sample revealed that the CNTs tend to bundle together, leading to an inhomogeneous dispersion of Pt nanoparticles (see inset in Fig. 6a). Thus, it is indicative that, in terms of Pt dispersion, CNT supports with larger diameters (preferably exceeding 3 nm) are loath to bundling and hence are more preferable as supports for the dispersion of metal catalyst, as evidenced by the particle size distribution profiles in Fig. 6.

The electrocatalytic performances of various Pt/C catalysts during MOR are shown in Fig. 7. All Pt/C samples displayed voltammograms associated with forward (I_f) and backward (I_b) anodic peak current densities within 0.4–0.7 V, which represent mass activity of catalyst and resistance toward catalyst deactivation (by coking) over the catalyst during MOR, respectively [11,12,57,58]. For comparison purpose, the observed I_f and I_b peak values are display in Table 2 along with the corresponding I_f/I_b ratio for various electrocatalysts. That the Pt/CNT-d3, Pt/CNT-d8, and Pt/CNT-d17 samples exhibited I_f/I_b ratios exceeding that of the Pt/SWCNT and the Pt/XC-72 indicates that Pt/CNT electrocatalysts with uniform diameters have higher electrocatalytic activities albeit all Pt/C samples have rather similar Pt loading as well as degree of graphitization (Table 2). The latter being inferred by the relative peak intensities of the D- and G-bands (i.e., the I_D/I_G ratio) derived from their respective Raman spectra. Electrocatalysts with a smaller I_D/I_G value thus have a better graphitization degree (i.e., more carbon with sp^3 than sp^2 structure), and presumably should have a better electrical conductivity. In other words, in view of the fact that all Pt/C samples have similar Pt loading and I_D/I_G ratios, the mass activity observed for various Pt/C electrocatalysts are mainly due to their diversities in Pt dispersion rather than the electrical characteristics (e.g., conductivities) of the carbon supports.

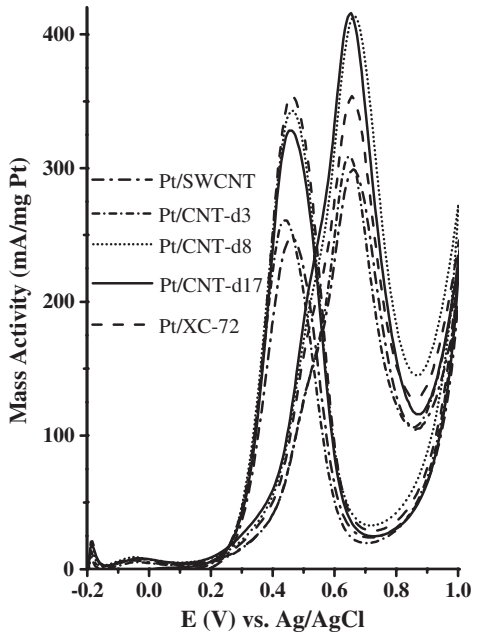

Fig. 7. Cyclic voltammograms of methanol oxidation for various Pt/C electrocatalysts.

The *EAS* values obtained for various Pt/C catalysts are also summarized in Table 2. These EAS values were derived based on the following equation:

$$EAS = \frac{Q_H}{[Pt] \times 0.21}$$

where [*Pt*] represents the Pt loading (in unit of mg/cm^3) in the electrode, the value 0.21 represents the charge required to oxidize a monolayer of H_2 on a fresh Pt surface [56], and Q_H is the Coulombic charge for hydrogen sorption in 1.0 M H_2SO_4 solution at room temperature between −0.2 and 1.0 V at a scanning rate of 10 mV/s. That higher *EAS* values were observed for the Pt/CNT-d3, Pt/CNT-d8, and Pt/CNT-d17 compared to the Pt/SWCNT and the Pt/Xc-72 samples indicates that these Pt/CNT catalysts with uniform diameters of MWCNT supports not only possess higher electrocatalytic performances during MOR but also better Pt dispersion, in line with the results obtained from TEM analyses. Indeed, it is known that a high dispersion and a narrow particle size distribution of noble metal nanoparticles are prerequisite in ensuring a high electrocatalytic performance of the catalyst [59]. Note that the I_f/I_b ratios obtained from Pt/CNTs appear to increase with increasing diameter of the CNT supports (Table 2), indicating that CNTs with larger diameters are not only more favorable for dispersion of Pt nanoparticles with uniform sizes, but also less vulnerable to deactivation and more tolerable towards CO poisoning during MOR.

Finally, the stability and durability of various Pt/C electrocatalysts were accessed by CA measurements under prolonged operation time (Fig. 8). The CA curves of various electrocatalysts were recorded with aqueous solution (1 M MeOH + 0.5 M H_2SO_4) at a fixed anodic potential of 0.6 V [60,61]. Typically, all electrocatalysts exhibit a rapid decrease in electrochemical activity during the initial period, followed by a gradual decrease with prolonged operation. Among them, the Pt/CNT-d8 and the Pt/CNT-d17 catalysts show the anticipated higher electrocatalytic

Table 2
Physicochemical properties and catalytic performances of various Pt/C electrocatalysts.

Catalyst	Metal content (wt.%)[a]		I_D/I_G[b]	I_f[c] (A/g of Pt)	I_r[c] (A/g of Pt)	I_f/I_r	*EAS* (m^2/g Pt)	Pt particle size[d] (nm)
	Fe	Pt						
Pt/CNT-d3	2.6	12.9	1.25	308	294	1.20	60	3.7
Pt/CNT-d8	4.8	9.3	1.25	413	321	1.22	68	2.4
Pt/CNT-d17	5.2	10.5	1.29	416	316	1.31	75	2.4
Pt/SWCNT	4.5	12.9	1.29	298	262	1.18	52	3.2
Pt/XC-72	–	12.5	1.39	353	349	1.01	47	2.5

[a] Pt loading measured by TGA analysis.
[b] Peak intensity ratio of D-band (sp^2 carbon) vs. G-band (sp^3 carbon) obtained from the Raman spectrum.
[c] Maximum current density of the forward (I_f) and reversed (I_r) scans during CV analyses.
[d] Pt particle size estimated by Scherrer formula [55] based on the large-angle XRD (220) diffraction peak of Pt metal at 2θ–68°.

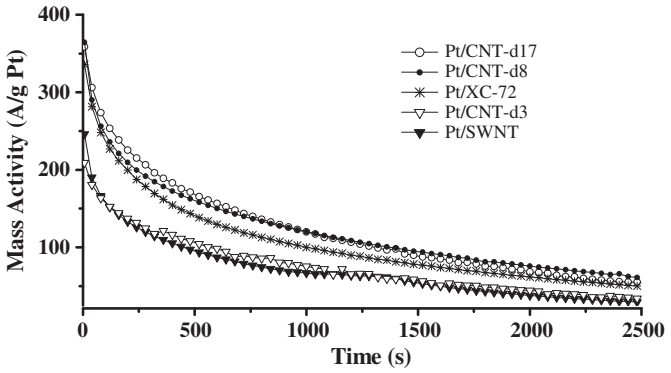

Fig. 8. CA curves for Pt/CNT-d17, Pt/CNT-d8, Pt/CNT-d3, Pt/SWCNT, and Pt/XC-72 samples in 0.5 M H_2SO_4 + MeOH at 0.6 V.

activity than the Pt/XC-72, in excellent agreement with the results obtained from EAS and CV measurements.

4. Conclusions

In summary, a series of Fe-containing hexagonal mesoporous silicas with varied pore sizes, which were prepared either by co-precipitation or impregnation method, have been employed to catalyze formation of CNTs *via* CVD process. It is found that by properly confining the metal catalyst in the mesoporous channels of the silica supports, multi-wall CNTs with uniform and controllable diameters may be facilely synthesized with high yield. The diameter of the MWCNTs is found to play a crucial role in the dispersion of Pt nanoparticles and the electrocatalytic performances of the resulting supported Pt/CNT catalysts during methanol oxidation reaction. These Pt/MWCNTs electrocatalysts, particularly those with diameter exceeding ca. 8 nm were found to exhibit electrocatalytic performances surpassing that of the conventional Pt/XC-72 and Pt/SWCNT catalysts having a similar Pt loading and electrochemical properties of the carbon supports.

Acknowledgment

The financial support of this work by the National Science Council, Taiwan (NSC98-2113-M-001-007-MY3 to SBL) is gratefully acknowledged.

References

[1] A. Roucoux, J. Schulz, H. Patin, Chem. Rev. 102 (2002) 3757.
[2] J.M. Thomas, B.F. Johnson, R. Raja, G. Sankar, P.A. Midgley, Acc. Chem. Res. 36 (2003) 20.
[3] W.M. Chen, G.Q. Sun, Z.X. Liang, Q. Mao, H.Q. Li, G.X. Wang, Q. Xin, H. Chang, C.H. Pak, D. Seung, J. Power Sources 160 (2006) 933.
[4] H. Chang, S.H. Joo, C. Pak, J. Mater. Chem. 17 (2007) 3078.
[5] P.V. Shanahan, L.B. Xu, C.D. Liang, M. Waje, S. Dai, Y.S. Yan, J. Power Sources 185 (2008) 423.
[6] F.J. Nores-Pondal, I.M.J. Vilella, H. Troiani, M. Granada, S.R. de Miguel, O.A. Scelza, H.R. Corti, Inter. J. Hydrogen Energy 34 (2009) 8193.
[7] H. Chang, S.H. Joo, C.H. Pak, J. Mater. Chem. 17 (2007) 3078.
[8] H.T. Kim, D.Y. You, H.K. Yoon, S.H. Joo, C.H. Pak, H. Chang, I.S. Song, J. Power Sources 180 (2008) 724.
[9] B. Fang, J.H. Kim, C. Lee, J.S. Yu, J. Phys. Chem. C 112 (2008) 639.
[10] E.P. Ambrosio, C. Francia, M. Manzoli, N. Penazzi, P. Spinelli, Inter. J. Hydrogen Energy 33 (2008) 3142.
[11] S.H. Liu, R.F. Lu, S.J. Huang, A.Y. Lo, S.H. Chien, S.B. Liu, Chem. Commun. 32 (2006) 3435.
[12] S.H. Liu, W.Y. Yu, C.H. Chen, A.Y. Lo, B.J. Hwang, S.H. Chien, S.B. Liu, Chem. Mater. 20 (2008) 1622.
[13] S.H. Liu, C.C. Chiang, M.T. Wu, S.B. Liu, Inter. J. Hydrogen Energy 35 (2010) 8149.
[14] X. Wang, W.Z. Li, Z.W. Chen, M. Waje, Y.S. Yan, J. Power Sources 158 (2006) 154.
[15] S.J. Guo, S.J. Dong, E. Wang, J. Phys. Chem. C 112 (2008) 2389.
[16] R.I. Jafri, N. Sujatha, N. Rajalakshmi, S. Ramaprabhu, Inter. J. Hydrogen Energy 34 (2009) 6371.
[17] H.Y. Du, Y.T. Tsai, C.P. Chen, C.J. Huang, L.C. Chen, K.H. Chen, H.C. Shih, J. Power Sources 171 (2007) 55.
[18] H.Y. Du, C.H. Wang, H.C. Hsu, S.T. Chang, U.S. Chen, S.C. Yen, L.C. Chen, H.C. Shih, K.H. Chen, Diamond Relat. Mater. 17 (2008) 535.
[19] Y. Mu, H. Liang, J. Hu, L. Jiang, L. Wan, J. Phys. Chem. B 109 (2005) 22212.
[20] W.Z. Li, C.H. Liang, W.J. Zhou, J.S. Qiu, Z.H. Zhou, G.Q. Sun, Q. Xin, J. Phys. Chem. B 107 (2003) 6292.
[21] J. Kong, M. Chapline, H. Dai, Adv. Mater. 13 (2001) 1384.
[22] H.C. Choi, M. Shim, S. Bangsaruntip, H. Dai, J. Am. Chem. Soc. 124 (2002) 9058.
[23] T. Nelson, K. Vinodgopal, G.G. Kumar, P. Kamat, Electrochem. Soc. Proc. 12 (2004) 152.
[24] C.J. Lee, S.C. Lyu, Y.R. Cho, J.H. Lee, K.I. Cho, Chem. Phys. Lett. 341 (2001) 245.
[25] C.H. Kuo, A. Bai, C.H. Huang, Y.Y. Li, C.C. Hu, C.C. Chen, Carbon 43 (2005) 2760.
[26] Y.C. Choi, Y.M. Ghin, Y.H. Lee, B.S. Lee, G.S. Park, W.B. Choi, N.S. Lee, J.M. Kim, Appl. Phys. Lett. 76 (2000) 2367.
[27] Y.Y. Wei, G. Eres, V.I. Merkulov, D.H. Lowndes, Appl. Phys. Lett. 78 (2001) 1394.
[28] W.Z. Li, D.Z. Wang, S.X. Yang, J.G. Wen, Z.F. Ren, Chem. Phys. Lett. 335 (2001) 141.
[29] N. Wang, Z.K. Tang, G.D. Li, J.S. Chen, Science 408 (2000) 50.
[30] N.D. Hoa, N.V. Quy, Y. Cho, D. Kim, Sens. Actuators B 127 (2007) 447.
[31] T. Kyotani, L.F. Tsai, A. Tomita, Chem. Mater. 8 (1996) 2109.
[32] I. Eswaramoorthi, L.P. Hwang, Diamond Relat. Mater. 6 (2007) 1571.
[33] S.H. Jeong, H.Y. Hwang, S.K. Hwang, K.H. Lee, Carbon 42 (2004) 2073.
[34] W.S. Im, Y.S. Cho, G.S. Choi, F.C. Yu, D.J. Kim, Diamond Relat. Mater. 13 (2004) 1214.
[35] I. Eswaramoorthi, L.P. Hwang, Carbon 44 (2006) 2341.
[36] B.D. Yao, N. Wang, J. Phys. Chem. B 105 (2001) 11395.
[37] J.S. Beck, J.C. Vartuli, W.J. Roth, M.E. Leonowicz, C.T. Kresge, K.D. Schmitt, C.T.W. Chu, D.H. Olson, E.W. Sheppard, S.B. McCullen, J.B. Higgins, J.L. Schlenker, J. Am. Chem. Soc. 114 (1992) 10834.
[38] D. Zhao, J. Feng, Q. Huo, N. Melosh, G.H. Fredrickson, B.F. Chmelka, G.D. Stucky, Science 279 (1998) 548.
[39] D. Zhao, Q. Huo, J. Feng, B.F. Chmelka, G.D. Stucky, J. Am. Chem. Soc. 120 (1998) 6024.
[40] Y. Wan, D. Zhao, Chem. Rev. 107 (2007) 2821.
[41] Y. Chen, L. Wei, B. Wang, S. Lim, D. Ciuparu, M. Zheng, J. Chen, C. Zoican, Y. Yang, G.L. Haller, L.D. Pfefferle, ACS Nano 1 (2007) 327.
[42] X.Q. Wang, M. Wang, H.X. Jin, Z.H. Li, P.M. He, Appl. Surf. Sci. 243 (2005) 151.
[43] T. Somanathan, A. Pandurangan, Appl. Surf. Sci. 254 (2008) 5643.
[44] Y. Chen, B. Wang, L.J. Li, Y. Yang, D. Ciuparu, S. Lim, G.L. Haller, L.D. Pfefferle, Carbon 45 (2007) 2217.
[45] Y. Murakami, S. Yamakita, T. Okubo, S. Maruyama, Chem. Phys. Lett. 375 (2003) 393.
[46] S. Lim, D. Ciuparu, C. Pak, F. Dobek, Y. Chen, D. Harding, L. Pfefferle, G. Haller, J. Phys. Chem. B 107 (2003) 11048.
[47] Y. Yang, J.D. York, J. Xu, S. Lim, Y. Chen, G.L. Haller, Micropor. Mesopor. Mater. 86 (2005) 303.
[48] D. Barreca, W.J. Blau, G.M. Croke, F.A. Deeney, F.C. Dillon, J.D. Holmes, C. Kufazvinei, M.A. Morris, T.R. Spalding, E. Tondello, Micropor. Mesopor. Mater. 103 (2007) 142.
[49] C.Y. Mou, P. Lin, Pure Appl. Chem. 72 (2000) 137.
[50] Y.J. Han, J.M. Kim, G.D. Stucky, Chem. Mater. 12 (2000) 2068.
[51] A.Y. Lo, S.J. Huang, W.H. Chen, Y.R. Peng, C.T. Kuo, S.B. Liu, Thin Solid Films 498 (2006) 193.
[52] M.H. Lim, A. Stein, Chem. Mater. 11 (1999) 3285.
[53] S. Jana, B. Dutta, R. Bera, S. Koner, Langmuir 23 (2007) 2492.
[54] L. Mercier, T.J. Pinnavaia, Adv. Mater. 9 (1997) 500.
[55] B.D. Cullity, Elements of X-ray diffraction, Second Ed., Addison-Wesely Publishing Co., 1978, pp. 100–102.
[56] A. Pozio, M. De Francesco, A. Cemmi, F. Cardellini, L. Giorigi, J. Power Sources 105 (2002) 13.
[57] Z. Liu, X.Y. Ling, X. Su, J.Y. Lee, J. Phys. Chem. B 108 (2004) 8234.
[58] J.N. Tiwari, F.M. Pan, R.N. Tiwari, S.K. Nandi, Chem. Commun. (2008) 6516.
[59] Y. Shao, J. Liu, Y. Wang, Y. Lin, J. Mater. Chem. 19 (2009) 46.
[60] J. Xu, K. Hua, G. Sun, C. Wang, X. Lv, Y. Wang, Electrochem. Commun. 8 (2006) 982.
[61] B. Rajesh, K. Ravindranathan Thampi, J.M. Bonard, A.J. McEvoy, N. Xanthopoulos, H.J. Mathieu, B. Viswanathan, J. Power Sources 133 (2004) 155.